Korean J. Chem. Eng., 35(4), 1045-1052 (2018)
DOI: 10.1007/s11814-017-0328-2

pISSN: 0256-1115
eISSN: 1975-7220

Morphological, acoustical, and physical properties of free-rising polyurethane foams depending on the flow directions

Giwook Sung, Hyeon Choe, Yeongsu Choi, and Jung Hyeun Kim†

Department of Chemical Engineering, University of Seoul, 163 Siripdaero, Dongdaemun-gu, Seoul 02504, Korea
(*Received 20 September 2017 • accepted 22 November 2017*)

Abstract−Polyurethane foam is widely used for automobile compartments as sound absorption materials due to its excellent noise dissipation characteristics. This sound absorption property is strongly dependent on the cavity and pore structures of the foams, and the cell morphology can be modulated by controlling experimental parameters. Two types of gelling catalysts were demonstrated in fabrications of polyurethane foams to control the cell morphology. The cell morphology of the free-rising polyurethane foams was investigated using dibutyltin-dilaurate and triethylenediamnine gelling catalysts, and the cell structures were analyzed from the free-rising samples obtained in various sampling heights and flow directions. The finer cell morphology was obtained with the organotin type catalyst by the faster gelling reactivity, compared with the amine type catalyst. In addition, the spherical small cavities in the samples obtained from horizontal planes of the free-rising foams revealed higher sound absorption coefficient and physical toughness than the elliptical irregular cavities from vertical planes, due to the higher homogeneity of cavity distributions in the horizontal planes.

Keywords: Polyurethane Foams, Flow Direction, Catalysts, Sound Absorption Coefficient

INDRODUCTION

Polyurethane foams have been commonly used as noise-controlling materials in the automobile industry because of their high sound absorption, light weight, and ease of production [1]. Generally, the two major automobile generated noises are structural-borne (30-500 Hz) and air-borne noise (500-8000 Hz) [2,3], and each propagates through solid and air media. Various studies have revealed that flexible polyurethane foams are advantageous for absorbing air-borne noise owing to their high damping in high frequencies resulting from their low density and high malleability [4,5]. Therefore, engine noise (1,600-4,000 Hz) [6] can be diminished by using polyurethane foams, and the foams are normally located on the inside as enclosures or in conjunction with barriers in the engine room. For this reason, the sound absorption coefficients at the high frequency region are important for improving performance. Generally, the sound absorption coefficient is associated with morphological properties because sound absorption is normally accomplished via sound energy dissipation as heat by collisions between air molecules and cell walls or mechanical frictions at sample boundaries [5,7-10].

To secure stable sound absorption of the foamed materials, it is important to have robust cellular structures of the polyurethane foams by designing homogeneous cavity distributions in the foams. Doutres et al. [11] reported on the relationship between non-acoustic parameters and the sound absorption coefficient of polyurethane foams, and Zhang et al. [12] studied the effect of interconnected porosity on sound absorption. There have also been several studies on the sound absorption coefficients of other porous materials such as polyolefin-based foams [13] and natural rubber foams [14]. Generally, all of these studies concentrated on obtaining the highest sound absorption coefficient at specific samples. However, obtaining high sound absorption behavior in a wide range of samples is crucial to guarantee industrial usage with stable reproducibility. Therefore, it is important to modulate the cellular structure of free-rising polyurethane foams in terms of the sampling locations and flow directions.

We investigated the relationship between cell morphology and physical properties of free-rising polyurethane foams by controlling gelling catalysts, which ultimately affect the initial gelling mechanisms. For examining the relative gelling reactivity between dibutyltin-dilaurate and triethylenediamnine catalysts, Fourier transformed infrared spectroscopy (FTIR) was used. The high gelling reactivity during formations of polyurethane foams leads to high matrix strength at early stage of reactions, and thus it helps develop a uniformly distributed fine cell morphology. In free-rising polyurethane foams, the cellular morphology is also a function of sampling height or flow direction, and so the effects of sampling locations and flow directions (horizontal, vertical) on cell structure were explored. During strain deformation, the stress values of polyurethane foams were also measured to provide a general guidance as a long term usage with energy absorption behavior, depending on the cell structures.

EXPERIMENTAL

1. Materials

Polyether polyol (KE-810, OH value: 28±2) with a weight-average molecular weight of 6,000 g/mol was obtained from KPX Chem-

†To whom correspondence should be addressed.
E-mail: jhkimad@uos.ac.kr

Table 1. Formulation details of the free-rising polyurethane foams

	Materials	Content (g)*
Polyol system	Alcohol (KE-810)	100
	Surfactant (L-3002)	1.3
	Chain extender (DEA)	0.6
	Blowing agent (H_2O)	4.0
	Blowing catalyst (BL11)	0.08
	Gelling catalyst**	0.72
Isocyanate (KW 5029/1C-B)		61.4

*NCO index is 1

**Dabco 33LV or DBTDL explained in the materials section

ical. An isocyanate mixture (KW 5029/1C-B, %NCO: 35±0.5, containing 78% 4,4′-methylenebis(phenyl isocyanate), 5% benzene 1,1-methylenebis(4-isocyanato) homopolymer, and 17% toluene diisocyanate) was obtained from BASF. A blowing catalyst (BL11, Air Products and Chemicals, 70% bis(2-dimethylaminoethyl) ether diluted with 30% dipropylene glycol) was used for blowing reactions with deionized water. Gelling catalysts Dabco 33LV (Air Products and Chemicals, 33% 1,4-diazabicyclo-octane (also called as triethylenediamine, TEDA) and 67% dipropylene glycol) and dibutyltin dilaurate (DBTDL, Sigma-Aldrich) were used to promote gelling reactions through urethane linkage formation. A silicon surfactant (L-3002, Momentive Corp.) and chain extender (diethanolamine (DEA), Sigma-Aldrich Co.) were applied for cell structure stabilization and enhancement of cross-linking reactions, respectively.

2. Sample Preparation

Polyurethane foams were manufactured using one-shot polymerization method in a free-rising fashion. Before mixing entire component mixtures, various polyol systems containing polyol, catalysts, cross-linking agents, blowing agents, and surfactant were weighed in a 400-mL paper cup (see Table 1), and they were mixed at 1,700 rpm for 20 min using a mechanical stirrer. Subsequently, the polyol mixtures were blended with pre-weighed isocyanate components for fabrications of polyurethane foams at 6,000 rpm for 10 s. After the final blending process, the mixtures were poured into an open cylindrical container (diameter: 75 mm, height: 250 mm), and all samples were kept at room temperature for 3 h to complete the reactions. The relative humidity was maintained at 50±10% and the average density of the polyurethane foams was approximately 45±5 kg/m^3. After completion of polymerizations, the foams were cut into appropriate specimens for morphological and physical measurements.

Fig. 1(a) shows a typical photograph of a free-rising polyurethane foam in the container, and Fig. 1(b) shows the sampling locations of the foam sample for property assessments. Samples were taken from three different heights (bottom, middle, top) in horizontal and vertical flow directions, as shown schematically in Fig. 1(c).

3. Characterization

3-1. Fourier Transform Infrared (FTIR) Analysis

An FTIR spectrometer (FTIR Frontier, PerkinElmer Inc.) with an attenuated total reflectance (ATR) module was used to analyze polymerization reactions qualitatively with four scans and 4 cm^{-1} resolution. The reaction mixtures were placed on the diamond crystal of the ATR accessory in order to obtain absorbance spectra during polymerization every 10 s for 1 h. In addition, the relative reactivity between Dabco 33LV and DBTDL catalysts on the gelling reactions was examined using carbonyl stretching bands at 1,730 cm^{-1} (free urethane) and 1,715 cm^{-1} (hydrogen bonded urethane), respectively, with respect to the invariable peak intensity at 2,970 cm^{-1} from the internal standard for the C-H stretching band. Relative quantities of increments in urethane linkages were obtained by combining those two intensity peaks as a function of reaction time.

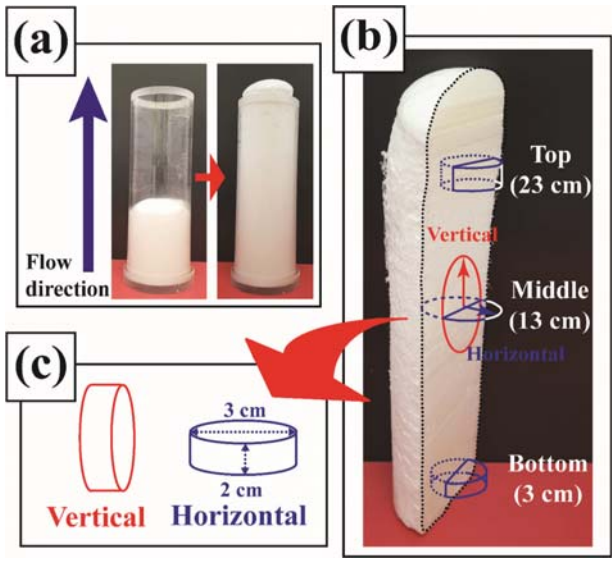

Fig. 1. A typical photograph showing free-rising process in a container (a), a cross-cut image of polyurethane foam for three different sampling locations (b), and two different samples depending on flow directions (c).

3-2. Morphology

The cellular structures of the polyurethane foams were examined using scanning electron microscopy (SEM, SNE-3000M, SEC Co. Ltd.) at 10 kV after the samples were treated with a gold film sputter (MCM 100, SEC Co. Ltd.). SEM images of the samples were collected from horizontal planes at the bottom, middle, and top heights as well as from a vertical plane at the middle height. At least 15 images for all polyurethane foams were analyzed using the Image Pro Plus software (Media Cybernetics Inc.) to obtain the average cavity and pore sizes and open porosities.

3-3. Physical Properties

The sound absorption coefficients of the polyurethane foams were measured using the impedance tube method (SW470, BSWA) with ASTM E1050-12, based on the transfer function method. The measurements were performed in the frequency range from 1,000 Hz to 6,300 Hz with two quarter-inch microphones. The thicknesses and diameters of cylindrical samples for measuring sound absorption coefficient were 20 and 30 mm, respectively. The stress-strain (SS) behavior of the polyurethane foams was examined using a dynamic mechanical analyzer (DMA, Q800, TA Instruments, USA) under compression mode, and also the cylindrical sample thickness and diameter for DMA measurements were 8 mm and

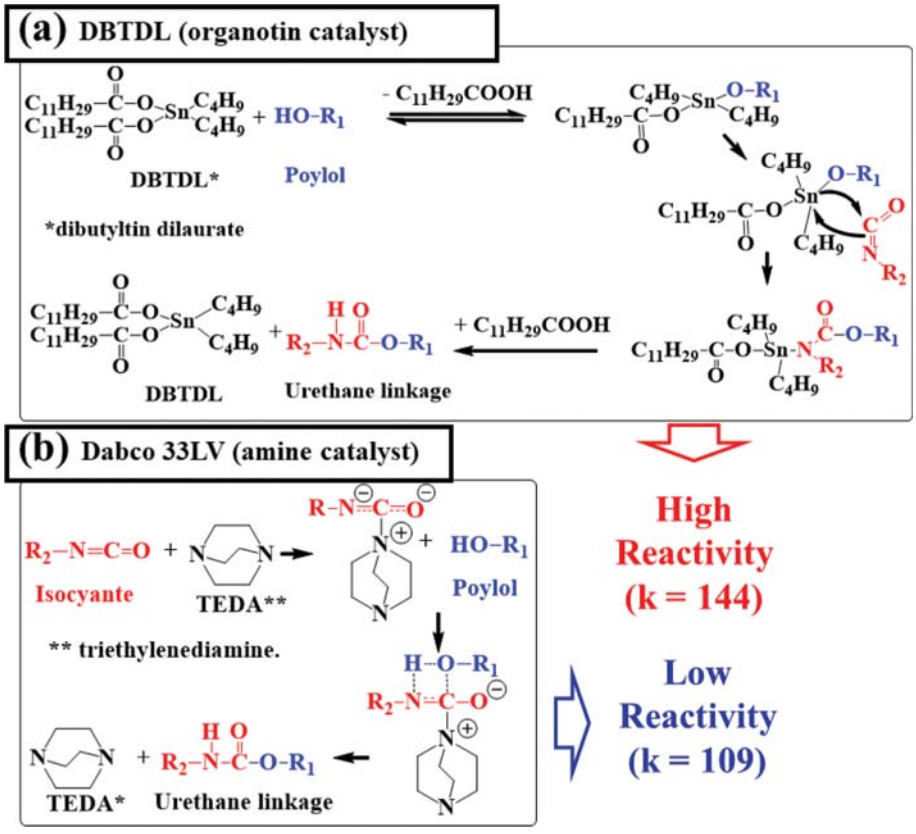

Fig. 2. Detailed reaction chemistry showing gelling reaction mechanisms with organotin DBTDL (a) and amine Dabco 33LV (b) catalysts.

20 mm. During the measurements, 3 N min^{-1} was applied as a stress rate, starting from the preloaded value of 0.05 N at room temperature.

RESULTS AND DISCUSSION

1. Reaction Mechanisms

Polyurethane main structure is produced from reactions between isocyanate and alcohol groups, and simultaneously the blowing agents (H_2O) generate CO_2 gas molecules by decomposing intermediate carbamic acid groups. In addition, final foam morphology and property are strongly governed by distributions of the gas molecules throughout the polyurethane matrix. Therefore, the gelling reaction on the polyurethane matrix is crucial for determining final foam properties. Fig. 2 shows the detail chemistry of polyurethane formation reactions using two different gelling catalysts. The gelling reaction is significantly improved by applying both organotin and amine catalysts. Fig. 2(a) reveals the role of the DBTDL tin catalyst in formation of polyurethane linkages. The OH functional group in polyol molecules replaces the long carbonyl acid chain in the DBTDL by nucleophilic addition, and then the replaced alkoxide complex further reacts with isocyanate groups to form carbamate linkage. Finally, the sterically unfavorable carbamate structure generates urethane linkages by returning to the original DBTDL structure. On the other hand, Fig. 2(b) also shows the reaction mechanism with the Dabco 33LV amine catalyst, as well-known as Baker's mechanism [15]. The first formed isocyanate complex with tertiary amine catalyst is attached by nucleophilic OH groups, and then the final complex also produces urethane linkages. Comparing the reaction rate constants for gelling reactions, the DBTDL (k=144 $L^2/g{\cdot}mol{\cdot}h$) shows faster reaction rate than that of Dabco 33LV (k=109 $L^2/g{\cdot}mol{\cdot}h$), which in turn the DBTDL results into the faster gelling performance over the Dabco 33LV [16].

To explore relative reaction rate with gelling catalysts, FTIR-ATR spectroscopy is used, as shown in several studies [17-19]. Extent of gelling reactions can be analyzed qualitatively using the absor-

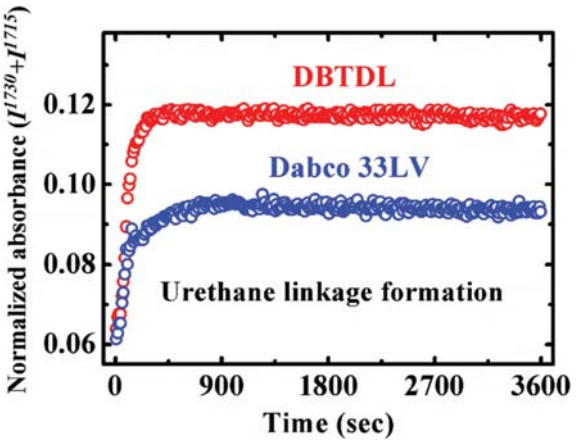

Fig. 3. Normalized peak absorbance with free and hydrogen bonded urethane linkages with DBTDL and Dabco 33LV catalysts from FTIR spectra.

bance intensity peaks from free urethane linkages and their hydrogen bonded interactions. Fig. 3 shows the normalized absorbance using 1,730 and 1,715 cm^{-1} peaks with respect to the invariable peak intensity at 2,970 cm^{-1} from the internal standard for the C-H stretching band. As demonstrated in Fig. 2 with gelling reaction chemistry, the DBTDL case revealed faster and higher urethane linkage formation than the Dabco 33LV case. This strong dependence of gelling catalysts on polyurethane reaction further impacts on the development of cavity and pore structure because the polyurethane matrix modulus is crucial in determining cell collapsing and growth mechanisms.

2. Cell Morphology

The cellular structures of the free-rising polyurethane foams were examined depending on the flow directions and sampling locations, as shown in Fig. 1. Recently, the effects of cellular structure of polyurethane foams on acoustic and physical properties have been widely reported [19-23]. The cellular properties such as cavity diameter, pore diameter, and open porosity are directly related to the sound absorption efficiency. Generally, the cavity and pore sizes play an important role in sound absorbing performance owing to complex mechanisms of sound wave collisions with the polyurethane matrix [5,8,10,12,24,25], and the open porosity also influences on the sound absorption behavior of the foams. In addition, fine and homogeneous cell structures are also advantageous in achieving robust physical properties.

Fig. 4 shows SEM images of polyurethane foams from different sampling locations in the horizontal planes with the Dabco 33LV and DBTDL gelling catalysts. Sampling locations represent the top, middle, and bottom of the foams from the bottom of the container, as shown in Fig. 1(c). Cavity sizes are smaller with the DBTDL catalyst than with the Dabco 33LV one, and the size uncertainty is also smaller in DBTDL case. In addition, homogeneity of cavity

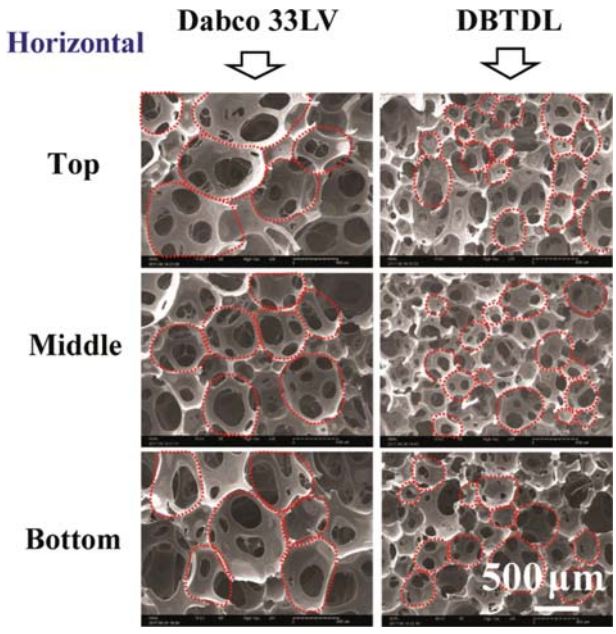

Fig. 4. SEM images of polyurethane foams sampled from three different locations with the Dabco 33LV and DBTDL catalysts.

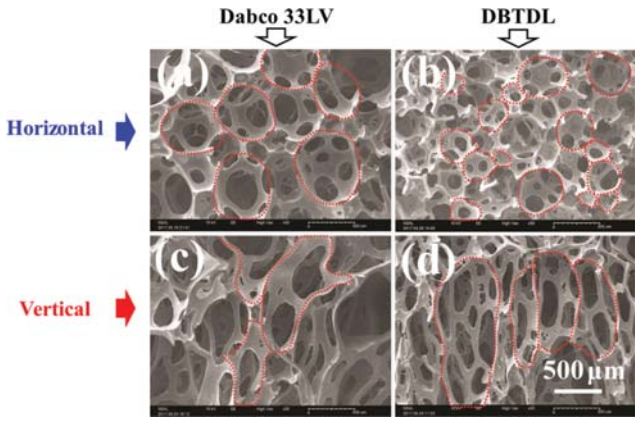

Fig. 5. SEM images of polyurethane foams sampled from horizontal and vertical planes at the middle height of the free-rising foams with the Dabco 33LV and DBTDL catalysts.

sizes depending on the sampling locations was much improved with the DBTDL catalyst regardless of the locations. However, the Dabco 33LV revealed much broader size distributions and higher variations in cavity sizes for different sampling locations. This homogeneous cavity size tendency with the DBTDL catalyst is primarily due to the high gelling reactivity, and its high gelling performance of polyurethane matrix leads to reduced cavity expanding and growth. Therefore, the gelling catalysts which have high reaction activity during urethane linkage formations can ensure homogeneous cellular structures and the reliable properties of polyurethane foams.

In addition to the effect of sample locations on the cell structure, the effect of flow directions on cavity and pore sizes in the free-rising foams was also examined in Fig. 5 with the two catalysts. In both types of catalysts, the cavity structure of the samples taken from horizontal planes was spherical shaped, but it showed an elliptical shape from the samples in vertical planes, regardless of the catalyst type. In addition, the cell morphology in the vertical sample with the Dabco 33LV revealed more irregular pattern than with the DBTDL. It can also be attributed to the higher collapsing phenomena between cavities with lower matrix resistance force due to the slower gelling reaction in applying the Dabco 33LV catalyst. As a result, this clear distinction of cell morphology depending on the flow directions can further influence the acoustic performance and physical properties of polyurethane foams.

By analyzing the cell morphologies using SEM images, Fig. 6 shows the mean cavity and pore diameters at three different sampling locations and depending on flow directions. As explained above in Figs. 4 and 5, average cavity and pore sizes were larger with the Dabco 33LV catalyst than with the DBTDL one at all three sampling locations, and also they showed larger values in vertically sampled cases for both catalysts. Again, it is the result of relative dominance between polyurethane matrix strength by gelling reaction and gases expansion pressure by blowing reaction. In this sense, higher gelling activity during polyurethane reaction can lead to stronger matrix modulus, and thus it provides less collapsing possibility of cavities at the same amount of gas generation (at the same amount of blowing agent).

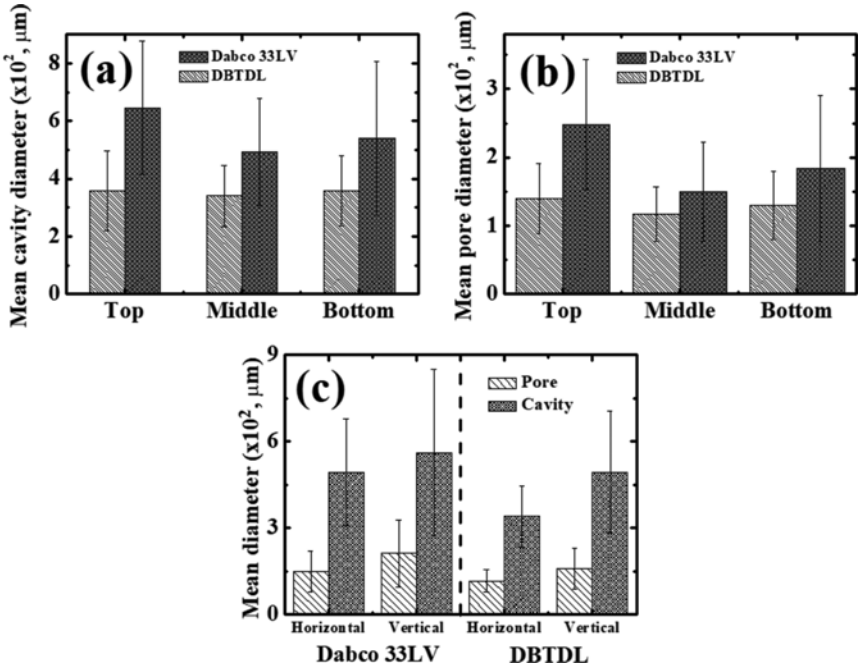

Fig. 6. Analysis of the mean cavity (a) and pore (b) diameters of polyurethane foams at three different sampling locations. Mean cavity and pore diameters with the horizontal and vertical plane samples (c).

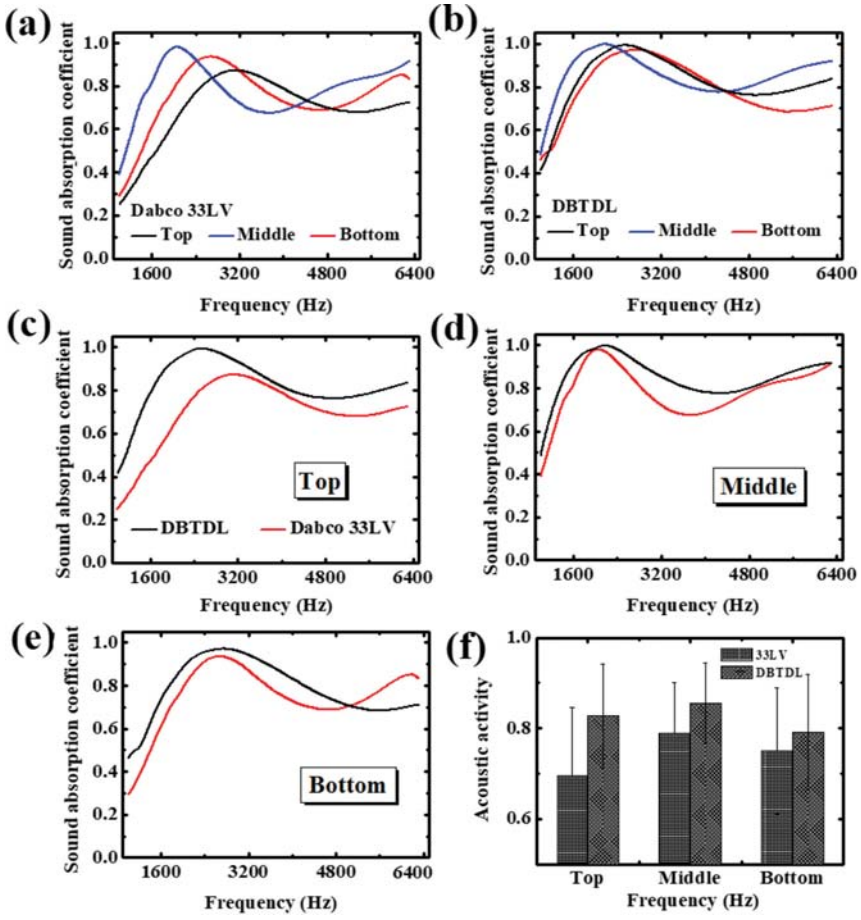

Fig. 7. Sound absorption coefficient of polyurethane foams with Dabco 33LV (a) and DBTDL (b) catalysts. Extracted sound absorption coefficients from (a) and (b) plots at top (c), middle (d), and bottom (e) sampling locations, and acoustic activities of the foams (f).

3. Acoustic Properties

The sound absorption coefficients of porous materials are generally affected by material parameters such as tortuosity, open porosity, airflow resistivity, and material modulus [26]. All these parameters are closely related to the sound absorption mechanisms like sound energy conversion to heat at sample boundaries [27], and these parameters have strong dependency on the cell morphology. Fig. 7 shows the results of sound absorption coefficients and acoustic activity from the polyurethane foam samples obtained at three different locations. The sound absorption coefficient with the Dabco 33LV catalyst varied with the sampling locations due to the variations of cellular morphology depending on the locations, as shown in Fig. 4. In addition, the smallest and relatively homogeneous cavity size distributions at the middle section resulted in the highest sound absorption coefficient in Fig. 7(a). However, the sound absorption coefficient with the DBTDL catalyst (in Fig. 7(b)) showed the similar level regardless of the sampling locations (in Fig. 7(c) through 7(e)) because of the uniform distributions of cavity sizes over the various locations. Also, its value was much higher than the case with the Dabco 33LV catalyst, and it is because the average cavity size is much smaller in the DBTDL case. Good distribution of high numbers of small cavity and pore is advantageous on energy dissipation by air molecular collisions with the cell walls. Acoustic activity, which is defined as the integrated area under the absorption coefficient curve [28], is useful for analyzing overall sound absorption efficiency of materials. Fig. 7(f) reveals the same tendency with the sound absorption coefficient results by applying both types of catalysts due to the clear morphological differences.

To compare the sound absorption coefficient depending on the morphological variations by flow directions, Fig. 8 shows the sound absorption coefficients and acoustic activity measured with the samples from horizontal and vertical planes for Dabco 33LV and DBTDL catalysts. Overall, sound absorption efficiencies obtained from the horizontal samples are higher than those from vertical samples, and this is mainly attributed to the clear difference in cellular morphology shown in Fig. 5. Homogeneously distributed spherical cavities could provide more efficient spaces for sound-wave dissipation than irregularly scattered elliptical cavities. In addition, again the DBTDL case showed better sound absorption performance over the Dabco 33LV case, as explained in Fig. 7. Therefore, in terms of designing cellular morphology in the free-rising polyurethane foams, it is very important to achieve high number of homogeneous spherical cavities in the foams for efficient sound absorbing instead of having irregularly distributed elliptical cavities.

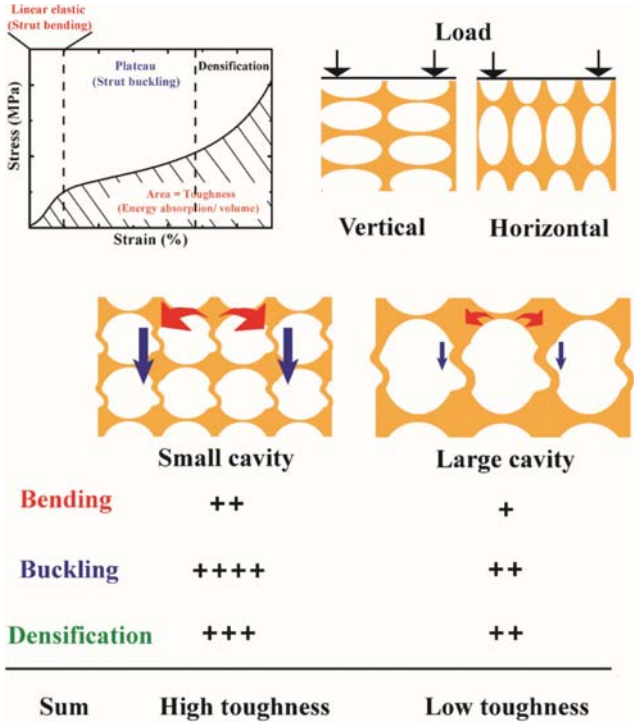

Fig. 9. Stress-strain behavior of foamed materials. Schematic illustrations showing cell morphologies for horizontal and vertical samples, and relative energy absorptions with small and large cavities.

4. Physical Properties

For applications of polyurethane foams as a sound-absorption material, physical properties are also crucial to guarantee not only long term usage but also stable performance. Generally, SS measurements under a compression mode are adopted for testing foam materials as a guidance of physical property. In an SS curve with foam-typed materials, there are three regions of deformation mechanisms (linear elastic, plateau, and densification), and those deformation regions are manifested by strut bending, buckling, and overall collapse [29]. Fig. 9 shows three regions of stress accumulation modes with increasing material strain, and the material tough-

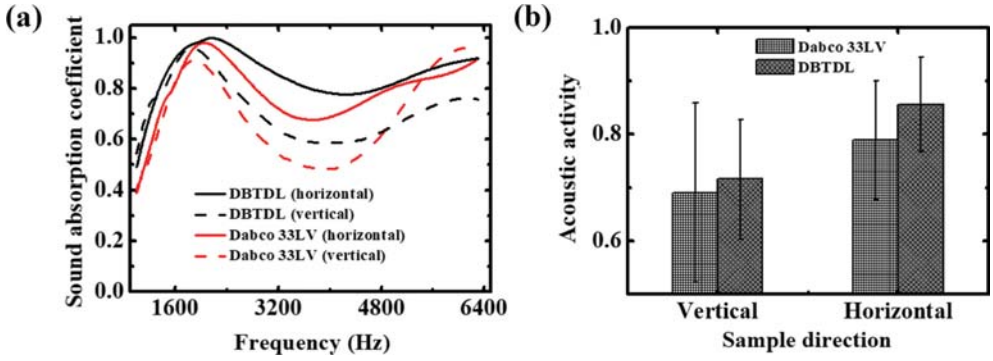

Fig. 8. Sound absorption coefficient (a) and acoustic activity (b) of polyurethane foams from horizontal and vertical flow directions.

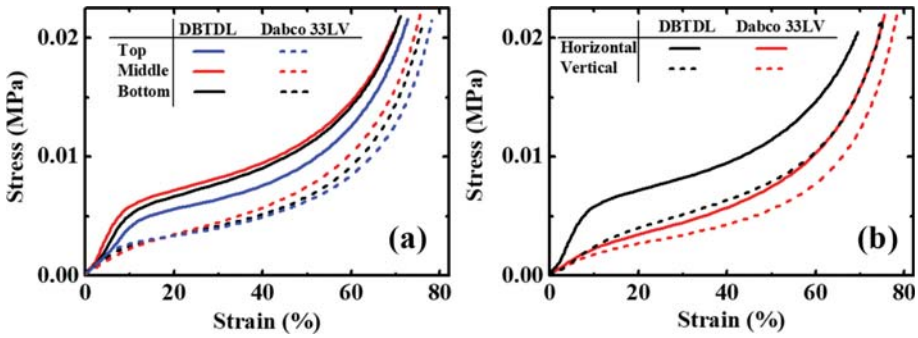

Fig. 10. Stress-strain plots of polyurethane foams with DBTDL and Dabco 33LV catalysts at three sampling locations (a), and the foams from horizontal and vertical planes (b).

ness can be estimated by integrating the SS curve. At the beginning of deformation, strut bending can be assigned for the linear elastic region, and then strut buckling is in charge of the following deformation through the long-side walls of the cavities. Finally, the cavities are totally compressed under densification mode with stiff stress increment. As shown in Fig. 9, the cavity arrangements are distinct depending on the flow directions, and they can play a critical role in the strut bending and buckling deformations. In addition, the cell walls in small cavity case absorb higher energy through strut bending and buckling processes during deformation than those in the large cavities, due to the large difference of cell wall populations. Therefore, as noted at the bottom of Fig. 9, the overall toughness can be much higher in the sample with small cavities than that with large cavities.

Fig. 10(a) shows the SS behavior of the samples manufactured with two types of catalysts at three different sampling locations, and Fig. 10(b) shows the effect of flow direction on SS curves. The foam samples with DBTDL catalyst reveal stronger linear elastic deformation region than with Dabco 33LV catalyst, and they also show higher plateau and densification stress. Overall, higher toughness of polyurethane foams at three different locations was obtained with DBTDL catalyst than with Dabco 33LV catalyst, and it is mainly due to the enhanced cell wall populations with homogeneously distributed small cavities, as demonstrated in Fig. 9. Additionally, the samples from the horizontal plane showed higher energy absorption in SS curves than from the vertical plane, regardless of the types of catalysts. It showed the strong dependency of cell morphology on flow direction, and the smaller cross-sectional area of the cavities in the horizontal plane produced higher stress values under strain than the larger cross-sectional area of the cavities in the vertical plane (see schematic diagram in Fig. 9). Therefore, the SS behavior is also strongly dependent on the cell morphology, and it is advantageous to have homogeneous small cavity distributions for improved toughness of foamed materials.

CONCLUSIONS

Free-rising polyurethane foams were fabricated by applying two types of gelling catalysts for designing fine cell morphology to improve sound absorption coefficients, and the cellular structure of polyurethane foams was examined for the two cases. FTIR-ATR spectroscopy was used to investigate the relative reaction rates of gelling catalysts, and the DBTDL case revealed faster and higher gelling reactivity than the Dabco 33LV case. Subsequently, this different gelling reactivity impacts on the final cell morphology. With high gelling reactivity in DBTDL case, the cavity and pore sizes were finer than Dabco 33LV case due to the relatively high polyurethane matrix strength developed by fast gelling reaction. Homogeneously distributed smaller spherical cavities showed higher sound absorption coefficient than the irregularly scattered larger elliptical cavities. The stress energy absorption during strain deformation was much improved with the smaller spherical cavities from the stress-strain measurements. Therefore, it is very advantageous to have homogeneously distributed small spherical cavities to achieve good sound absorption in various acoustic environments and high toughness of material deformations under applied forces.

ACKNOWLEDGEMENT

This work was supported by the 2017 Research Fund of the University of Seoul.

REFERENCES

1. L. J. Lee, C. Zeng, X. Cao, X. Han, J. Shen and G. Xu, *Compos. Sci. Technol.*, **65**, 2344 (2005).
2. N.-C. Park, Y.-C. Kim and C.-R. Park, *J. Korean Ind. Eng. Chem.*, **8**, 197 (1997).
3. J. J. Zwinselman and W. D. Bachmann, *J. Cell. Plast.*, **24**, 274 (1988).
4. D. K. Lee, L. Chen, A. Sendijarevic, V. Sendijarevic, K. C. Frisch and D. Klempner, *J. Cell. Plast.*, **27**, 135 (1991).
5. R. Gayathri, R. Vasanthakumari and C. Padmanabhan, *Int. J. Sci. Eng. Res.*, **4**, 301 (2013).
6. Y. Liu, Y. B. Jia, X. J. Zhang, Z. C. Liu, Y. C. Ren and B. Yang, *Appl. Mech. Mater.*, **307**, 196 (2013).
7. O. Doutres, N. Atalla and K. Dong, *J. Appl. Phys.*, **110**, 064901 (2011).
8. J. G. Gwon, S. K. Kim and J. H. Kim, *Mater. Des.*, **89**, 448 (2016).
9. J. G. Gwon, S. K. Kim and J. H. kim, *J. Porous Mater.*, **23**, 465 (2016).
10. C. H. Sung, K. S. Lee, K. S. Lee, S. M. Oh, J. H. Kim, M. S. Kim and H. M. Jeong, *Macromol. Res.*, **15**, 443 (2007).
11. O. Doutres, N. Atalla and K. Dong, *J. Appl. Phys.*, **113**, 054901

(2013).
12. C. Zhang, J. Li, Z. Hu, F. Zhu and Y. Huang, *Mater. Des.*, **41**, 319 (2012).
13. M. Álvarez-Láinez, M. A. Rodríguez-Pérez and J. A. de Saja, *Mater. Lett.*, **121**, 26 (2014).
14. S. Tomyangkul, P. Pongmuksuwan, W. Harnnarongchai and K. Chaochanchaikul, *J. Reinf. Plast. Compos.*, **35**, 688 (2016).
15. D. Randall and S. Lee, The polyurethanes book, Wiley, New York (2002).
16. E. Delebecq, J.-P. Pascault, B. Boutevin and F. Ganachaud, *Chem. Rev.*, **113**, 80 (2012).
17. G. Sung, J. G. Gwon, and J. H. Kim, *J. Appl. Polym. Sci.*, **133**, 43737 (2016).
18. J. G. Gwon, G. Sung and J. H. Kim, *Int. J. Precis. Eng. Manuf.*, **16**, 2299 (2015).
19. G. Sung, J. W. Kim and J. H. Kim, *J. Ind. Eng. Chem.*, **44**, 99 (2016).
20. G. Sung, S. K. Kim, J. W. Kim and J. H. Kim, *Polym. Test.*, **53**, 156 (2016).
21. S. K. Kim, G. Sung, J. G. Gwon and J. H. Kim, *Int. J. Precis. Eng. Manuf.-Green Technol.*, **3**, 367 (2016).
22. G. Sung and J. H. Kim, *Korean J. Chem. Eng.*, **34**, 1222 (2017).
23. G. Sung and J. H. Kim, *Compos. Sci. Technol.*, **146**, 147 (2017).
24. J. Lee, G. H. Kim and C. S. Ha, *J. Appl. Polym. Sci.*, **123**, 2384 (2012).
25. H.-M. Park, A. K. Mohanty, L. T. Drzal, E. Lee, D. F. Mielewski and M. Misra, *J. Polym. Environ.*, **14**, 27 (2006).
26. D. L. Johnson, J. Koplik and R. Dashen, *J. Fluid Mech.*, **176**, 379 (1987).
27. J. Allard and N. Atalla, Propagation of sound in porous media: modelling sound absorbing materials, John Wiley & Sons, Chichester (2009).
28. R. Verdejo, R. Stämpfli, M. Alvarez-Lainez, S. Mourad, M. Rodriguez-Perez, P. Brühwiler and M. Shaffer, *Compos. Sci. Technol.*, **69**, 1564 (2009).
29. J. A. Elliott, A. H. Windle, J. R. Hobdell, G. Eeckhaut, R. J. Oldman, W. Ludwig, E. Boller, P. Cloetens and J. Baruchel, *J. Mater. Sci.*, **37**, 1547 (2002).